Journal Pre-proof

Thermochemical stability of delafossite and other relevant ternary phases in the Cu–Fe–S–O–H system

Andrea Aquino, Marco Lezzerini, Andrea Giaccherini, Giordano Montegrossi, Francesco Di Benedetto

PII: S0883-2927(20)30287-0

DOI: https://doi.org/10.1016/j.apgeochem.2020.104795

Reference: AG 104795

To appear in: *Applied Geochemistry*

Received Date: 21 May 2020

Revised Date: 22 October 2020

Accepted Date: 23 October 2020

Please cite this article as: Aquino, A., Lezzerini, M., Giaccherini, A., Montegrossi, G., Di Benedetto, F., Thermochemical stability of delafossite and other relevant ternary phases in the Cu-Fe-S-O-H system, *Applied Geochemistry*, https://doi.org/10.1016/j.apgeochem.2020.104795.

Thermochemical stability of delafossite and other relevant ternary phases in the Cu-Fe-S-O-H system

Andrea Aquino[1], Marco Lezzerini[1], Andrea Giaccherini[2,3,*], Giordano Montegrossi[4] and Francesco Di Benedetto[3]

[1]Department of Earth Sciences, University of Pisa, Via S. Maria, 53, 56126, Pisa, Italy; andrea.aquino@phd.unipi.it; marco.lezzerini@unipi.it;

[2]Department of Industrial Engineering, University of Florence, Via S. Marta, 3, 50139, Florence, Italy; andrea.giaccherini@unifi.it;

[3]Department of Earth Sciences, University of Florence, Via G. La Pira 4, 50121, Florence, Italy; francesco.dibenedetto@unifi.it;

[4]National Research Council, Institute for Geosciences and Georesources, Via G. La Pira 4, 50121, Florence, Italy; montegrossi@igg.cnr.it;

*corresponding author

Abstract

In the present study the stability of the phases pertaining to the Cu-Fe-S-O-H compositional system is investigated using the Eh-pH prevalence diagrams. Calculations were performed under the PHREEQC formalism, simultaneously accounting for all concurrent equilibria. Accordingly, point-to-point mass balance diagrams were realised, changing initial parameters to explore the dependence of the system on the temperature, and on the metal-to-sulfur ratio. Among the most relevant results, discussed in comparison with the previous existing literature mainly driven by calculation performed under the so-called line method approximation, the occurrence of large field of stability of the ternary species (and, among them, of delafossite, $CuFeO_2$) and the net change of some boundaries in the stability fields of the binary species, due to competing equilibria. The results have been discussed on the light of the occurrence of these minerals in cuprous and ferrous mineralizations, and in the perspective of possible application in Corrosion Science.

1 Introduction

Minerals pertaining to the Cu-Fe-S-O-H compositional system are outermost relevant in the global society. From an industrial perspective, Copper and Iron extractions amount, respectively, at 21 million tons and 1.5 billion tons in 2018, this latter by far the most relevant extraction activity of a metal ore (USGS, 2018).

Copper and iron sulfides are widespread minerals often occurring in mineral assemblage such as, among others, Cu_xS-bornite ($1.5<x<2$), chalcopyrite-pyrite-bornite and chalcocite-pyrite (Crerar and Barnes, 1976). Most of them are used in the mineral industry to extract Cu or, as in the case of pyrite, it is exploited in the production of SO_2. From a technological perspective, these compounds are interesting as they can be employed as semiconductors in different field such as detectors, photovoltaics and thermoelectrics (Rockett, 2010; Siebentritt, 2017; Long et al., 2018), or battery technology (Qiu et al., 2014). This is mainly due to the peculiar properties exhibited by some of these phases: chalcocite (Cu_2S) is a superionic conductor at 104 °C (Miller et al., 2013), covellite (CuS) has been highlighted for its low temperature superconducting properties (Di Benedetto et al., 2006), chalcopyrite and bornite couple semiconducting and magnetic properties (Rais et al., 2000; Borgheresi et al., 2007). Cu and Fe oxides have attracted the interest of researchers since they are promising candidate for photoelectrochemical application, such e.g. water splitting and reforming of CO_2 (Takata et al., 1998; Read et al., 2012; Kang et al., 2015; Prévot et al., 2015). Indeed, they are more stable than sulfides when exposed to light absorption or under oxidative stress (Díaz-García et al., 2015; Su et al., 2017).

On the other hand, binary and ternary oxides of Cu and Fe have been largely studied also in the field of Corrosion Science, being involved in metals corrosion and/or mineral oxidation (Beverskog and Puigdomenech, 1997; Refait et al., 1998; Beverskog and Puigdomenech, 1999; Cook and Olive, 2012; concerning Fe, and Cubicciotti, 1988; Pourbaix, 1991; Beverskog and Puigdomenech, 1997; concerning Cu).

Within this context, delafossite, $CuFeO_2$, belongs to a peculiar situation. Delafossite is a very common mineral often occurring as alteration of ternary sulfides or reaction of CuO_x/FeO_y in a mixture (Anthony et al., 1997). The delafossite stability field does not appear in any Eh-pH diagram calculated by the equilibrium line method (Sato, 1992; Huang, 2016). Sato and Huang (Sato, 1992; Huang, 2016) suggested a possible Cu-Fe mixed phase, in certain regions where both elements exhibit superimposed predominance fields of the related binary oxides. Cubicciotti (1988) indicated a predominance field of

delafossite, although within the limits of the approximated line method approach. This field appeared confined within the 2/10 pH range, and the -0.2/0.5 V Eh range. Elsewhere, we showed how a point-by-point mass balance approach could clarify the stability of oxides or sulfides in the Cu-Sn-S-O-H compositional field (Giaccherini et al., 2016). Under this approach, the relationships between all phases of the compositional field (in equilibrium with an aqueous solution) in the Eh-pH diagrams are simultaneously studied. This method is commonly applied to describe the corrosion of metals in the Cu-Fe-S-O-H system, which is well described by the interaction of the solid surfaces with the aqueous films above them (whose thickness depend on the humidity). Within similar assumptions, we can also describe the alteration process of the different minerals, which follow their thermochemical stability. This marks an equivalence among the products of metal corrosion and the products of minerals alteration. However, presently some issues needs to be addressed: 1) a comprehensive review of the literature in the context of thermodynamic modelling and 2) a calculation of the Eh-pH diagram under the mass balance and point-by-point approach. For these reasons, we present a new thermochemical modelling of the quaternary system Cu–Fe–S–O better describing the natural occurrence of ternary phases.

2 Methods

2.1 State of the art on the Cu-Fe-S-O compositional field

2.1.1 Oxides

The most common binary Cu bearing oxide is cuprite (monoclinic Cu_2O). This phase usually occurs as secondary mineral forming by the oxidation of copper sulfide minerals. Similarly, tenorite (monoclinic CuO) occurs in the weathered or oxidized zone associated with deeper primary copper sulfide ore bodies and it is less common (Vaughan, 2006; Lafuente et al., 2015). Indeed, cuprite and tenorite are often associated in ores with native copper, azurite, chrysocolla, malachite and a variety of iron oxide minerals (Klein et al., 1985).

The stable iron oxides at room temperature conditions are: wustite (cubic FeO), hematite (trigonal α-Fe_2O_3), magnetite (cubic Fe_3O_4) and maghemite (cubic γ-Fe_2O_3). Wustite, hematite and magnetite are primary minerals, whereas maghemite occurs as a secondary mineral product of the magnetite alteration (Anthony et al., 1997). When the pressure is increased to the level of the deep mantle, other phases occur such as FeO_2 (cubic, pyrite-type) (Hu et al., 2016). On the other hand, the mixed valence

oxides at high pressure (Table 1) reveal an underlying structural complexity with several solubility lacunas among the phases. Still, three of them (Fe_5O_6, Fe_4O_5 and Fe_3O_4) share several structural features (Table 1).

Table 1 – High pressure iron binary oxides reported in the literature.

Formula	**Fe/O**	**Lattice**	**Conditions**	**Ref.**
Fe_5O_6	0.83	*Orthorhombic*	*HP*	(Lavina and Meng, 2015)
Fe_4O_5	0.80	*Orthorhombic*	*HP*	(Lavina et al., 2011)
$Fe_{25}O_{32}$	0.78	*Hexagonal*	*HP*	(Bykova et al., 2016)
Fe_3O_4	0.75	*Orthorhombic*	*HP*	(Dubrovinsky et al., 2016)
Fe_5O_7	0.71	*Monoclinic*	*HP*	(Bykova et al., 2016)
$Fe_{13}O_{19}$	0.68	*Monoclinic*	*HP*	(Merlini et al., 2015)

Since the phases in Table 1 occurs in the high-pressure range we did not include them in the thermodynamic database used for the calculations operated in this paper.

Differently from Cu-bearing phases (for which only the rare spertiniite $Cu(OH)_2$ is described), the Fe-bearing hydroxides commonly occur as alteration of iron-rich ores, and as relevant components of soils. Among them, goethite (orthorhombic α-FeO(OH)) and ferrihydrite (hexagonal cryptocrystalline $5Fe_2O_3{\cdot}9H_2O$, (Chukhov et al., 1974) are, by far, the most common. Limonite ($FeO(OH){\cdot}nH_2O$), is a very well-known mineraloid, once identified as mineral, but now recognized as a mixture of related hydrated iron oxide minerals, among them goethite, akageneite, monoclinic β-FeO(OH), lepidocrocite, orthorhombic γ-FeO(OH), and jarosite, $KFe_3(SO_4)_2(OH)_6$ (Hu et al., 2016).

The most naturally relevant ternary Cu-Fe oxide is delafossite (trigonal $CuFeO_2$) (Marquardt et al., 2006). Delafossite is a widespread mineral, often occurring as secondary mineral in deep oxidized areas of copper deposits (Anthony et al., 1997; Marquardt et al., 2006; Manutcher-Danai, 2009). Delafossite is often found as massive, relatively distinct crystals on hematite (Rogers, 1913). As material, due to a p-type semiconducting bandgap of 1.47 eV, is considered highly attractive for photovoltaic and for photoelectrochemical applications, as cathode for solar water splitting, and in lithium batteries. Delafossite is easily synthesized through solid state reactions of cuprous and ferric oxides as well as of sol-gel methods and hydrothermal syntheses (Mugnier et al., 2006; Benreguia et al., 2015; Sheets et al.

2006). In literature, two other ternary oxide phases have been discussed: cubic $CuFe_2O_4$ (cuprospinel or cuproferrite -) and Cu_2FeO_4. The former is a rare mineral only found in the consolidated Rambler mines limited near Baie Verte (Newfoundland) (Anthony et al., 1997), whereas the latter is rarely discussed, and never in natural occurrences (Cubicciotti, 1988; Mulafa-Bafubiandi, 2006).

2.1.2 Sulfur bearing phases

In the Cu-S compositional field, whose endmember are CuS (covellite) and Cu_2S (chalcocite), several structurally related phases are present (crystalline: anilite, Cu_7S_4, digenite, Cu_9S_5, djurleite, $Cu_{31}S_{16}$; cryptocrystalline: geerite Cu_8S_5, yarrowite, Cu_9S_8, and spionkopite $Cu_{39}S_{28}$; Goble, 1985). These phases share common structural blocks, being differentiated by minimal stoichiometric changes and 3D stacking features. Accordingly, they can be often found intimately associated in mineral ores (Whiteside and Goble, 1986; Gablina et al., 2006). Oxidation of Cu bearing sulfides deposits is often associated with the emergence of hydrated or basic sulfates, among which brochantite (tetragonal $Cu_4(SO_4)(OH)_6$), antlerite, (orthorhombic $Cu_3(SO_4)(OH)_4$), chalcanthite, triclinic $CuSO_4.5H_2O$, boothite, monoclinic $CuSO_4.7H_2O$, bonattite, monoclinic $CuSO_4.3H_2O$, can be mentioned (Anthony et al., 1997).

Stable binary non-stochiometric iron sulfides are generally referred as pyrrhotites ($Fe_{1-x}S$, $0<x<0.2$), defective species structurally related to the planetary troilite (hexagonal FeS) mineral (Vaughan and Craig, 1978. Other stable iron-sulfides are mackinawite (tetragonal FeS), pyrite (cubic FeS_2), and its polymorph, marcasite (orthorhombic FeS_2) (Klein et al., 1985). Several Fe sulfates have been described in the literature. Among them, the most common occurrences are reported for melanterite $FeSO_4.7H_2O$, amarantite $Fe_2(SO_4)_2O.7H_2O$ e coquimbite $Fe_2(SO_4)_3.9H_2O$ (Fang and Robinson, 1970).

Among all ternary Cu-Fe-S phases, chalcopyrite ($CuFeS_2$ – tetragonal) and bornite (Cu_5FeS_4 - orthorhombic) are the most common in ores. Idaite (Cu_5FeS_6 – tetragonal) is a secondary mineral often occurring through the enrichment of the isostructural chalcopyrite or through lamellar decomposition of bornite (Hatert, 2004). Other stable ternary sulfides at room temperature and pressure fukuchilite Cu_3FeS_8, talnakhite $Cu_9(Fe,Ni)_8S_{16}$, mooihoekite $Cu_9Fe_9S_{16}$, haycockite $Cu_8Fe_{10}S_{16}$ and nukundamite $(Cu,Fe)_4S_4$ (Raghavan, 2004). The only mixed sulfate phase worth to be mentioned is cuprocopiapite, triclinic $CuFe_4(SO_4)_6(OH)_2 \cdot 20H_2O$, a rare phase associated to alteration of Cu and Fe oxyhydroxides and sulfate phases (Bandy, 1938).

2.2 Modelling of the equilibria in aqueous solutions

We chose to study the stability of the different species, by the element specific predominance charts. In these diagrams, we identified the predominant species for each element as the ones having the highest amount at the equilibrium. The amount of a species is the absolute element content (in moles) considering both aqueous and solid species (Huang, 2016). The element specific predominance charts can be directly compared to the line equilibrium Eh-pH diagrams available in literature, usually computed for chemical environment with a single metal. Accordingly, the analyses illustrated in the next paragraph will focus on the copper and iron predominance charts, separately.

Calculations were performed under the PHREEQC formalism, simultaneously accounting for all concurrent equilibria in the Cu-Fe-S-O-H system, for a grid of (Eh, pH) values, and keeping fixed other parameters such as temperature and pressure. This approach is generally known as point-by-point mass balance calculation (Parkhurst and Appelo, 1999; Huang, 2016). A reference database file accounts for equilibria involving aqueous species, gaseous species and solid phases through aqueous equilibria or dissolution/precipitation reactions. The entries in the database reports the stability of the chemical species as the logarithm of equilibrium constant (log K). These equilibria refer to the reaction of the master species to form all other chemical species (Johnson et al., 1992; Parkhurst and Appelo, 1999). The database includes dissolution reactions (e.g. $O_2(g) = O_2(aq)$) and the corresponding equilibrium. To realise the grid, we set up computation at different constrained Eh and pH values. Accordingly, the software computed all the corresponding equilibria and speciation. Activities of the different species were calculated according to the B-dot standard model, i.e. an extended Debye-Huckel activity model (Parkhurst and Appelo, 1999). The PHREEQC wateq4f.dat database (Ball and Nordstrom, 1991; Berger et al., 2011), upgraded by the phases added by Giaccherini et al. (2016), already included the thermodynamic properties of most chemical species relevant to our model. Additional phases were added to the database for the purposes of the present calculation: troilite, FeS, cubanite, Cu_2FeS_3, and bornite, Cu_5FeS_4, whose thermodynamic data were reported by Helgeson et al. (1978). We checked for delafossite thermodynamic data, already present in the wateq4f.dat standard database, and upgraded it with what of Kang et al. (2015) reported. To verify the reliability of the chosen model, we calculated also the Fe-O-H and Fe-S-O-H diagrams and comparing them with the literature diagram (Huang 2016) we did not evidence significant differences.

In the following, we use the expression “total concentration of a chemical element” (e.g. [Cu]) referring to the total mass of all species bearing a certain chemical element. In the present study, we calculated Eh-pH data under the following conditions:

1) [S]=1 10^{-1} mol dm^{-3}, [Fe]=[Cu] = 1 10^{-6} mol dm^{-3}, T =293 K
2) [S]=1 10^{-1} mol dm^{-3}, [Fe]=[Cu] = 1 10^{-3} mol dm^{-3}, T =293 K
3) [S]=1 10^{-1} mol dm^{-3}, [Fe]=[Cu] = 1 10^{-3} mol dm^{-3}, T =373 K
4) [S]=1 10^{-1} mol dm^{-3}, [Fe]=[Cu] = 1 10^{-3} mol dm^{-3}, T =473 K

Accordingly, the effects of metal concentration and of temperature can be studied. All the predominance charts are computed in 100x100 points grid in the Eh-pH space.

3 Results

3.1 Copper-bearing species

In **Figures 1a and 1b**, the predominance charts relative to the Cu species only are shown. Calculations have been limited by both the hydrogen evolution reaction (HER) on the reducing side (low Eh) and the oxygen evolution reaction (OER) on the oxidising side (high Eh). Calculations performed assuming low (10^{-6} mol dm^{-3}) and high (10^{-3} mol dm^{-3}) metal concentration are plotted in the **Figures 1a and 1b**, respectively.

In the low concentration regime (**Fig. 1a**), the diagram is dominated by solid phases (sulfides and elemental Cu) under reducing conditions, and by species in solutions (Cu^{2+}, hydrated $Cu(OH)_2$ and $Cu(OH)_4^-$) under oxidising conditions. However, the most relevant feature is represented by the predominance field of delafossite, which appears by far the widest of the whole diagram.

In the high concentration regime (**Fig. 1b**), only modest differences are achieved. The stabilisation of solid phases occurs, well testified by the replacement of the fields of $Cu(OH)_2$ and $Cu(OH)_4^-$ by those of brochantite and tenorite. Similarly, the delafossite fields increases at the expenses of the Cu^{2+} field, as well as that of chalcopyrite increases at the expenses of the fields of the Cu sulfides.

The predominance charts shown in the **Figures 2a an 2b** show the effect of temperature on the stability of the main phases present in the high concentration regime only. The most relevant difference with respect to the predominance chart at room temperature (**Fig. 1b**) is the smaller number of predominant phases. Brochantite and anilite have no more a predominant field at 373 K (**Fig. 2a**), whereas the chalcocite predominance field decreases at 373 K and vanishes from the Eh-pH diagram at 473 K (**Fig. 2b**). On the contrary, the predominance fields of covellite and delafossite, and at a lower extent, of tenorite increase at 373 K and even more at 473 K.

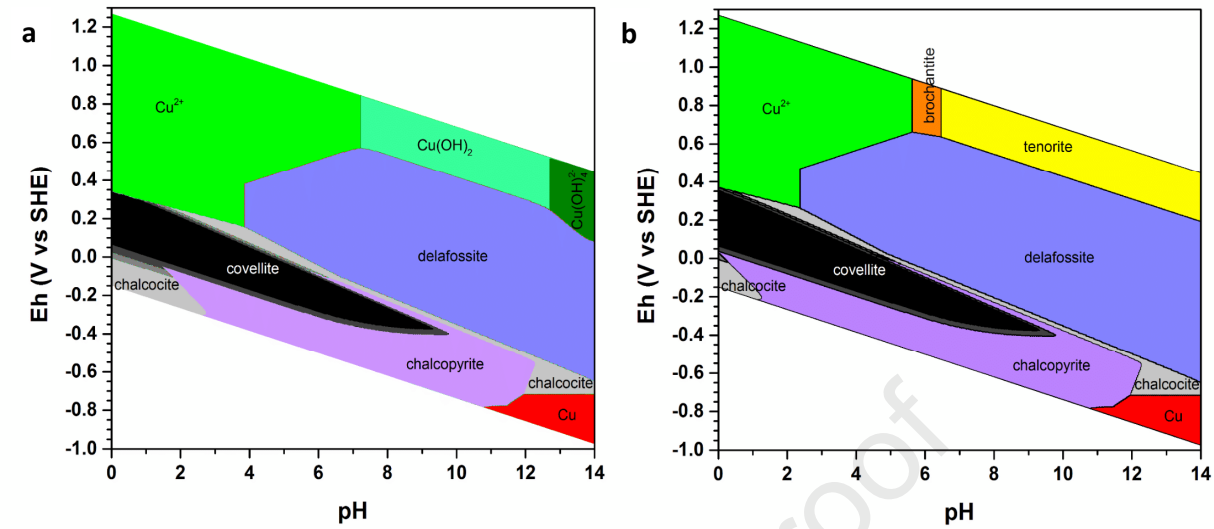

Figure 1 – Eh-pH prevalence diagrams presenting Cu-bearing species at 293 K for [S]=1 10^{-1} mol dm^{-3} a) [Cu]=[Fe]=1 10^{-6} mol dm^{-3} and b) [Cu]=[Fe]=1 10^{-3} mol dm^{-3}. Additional regions present in the diagrams: djurleite (grey), anilite (dark grey)

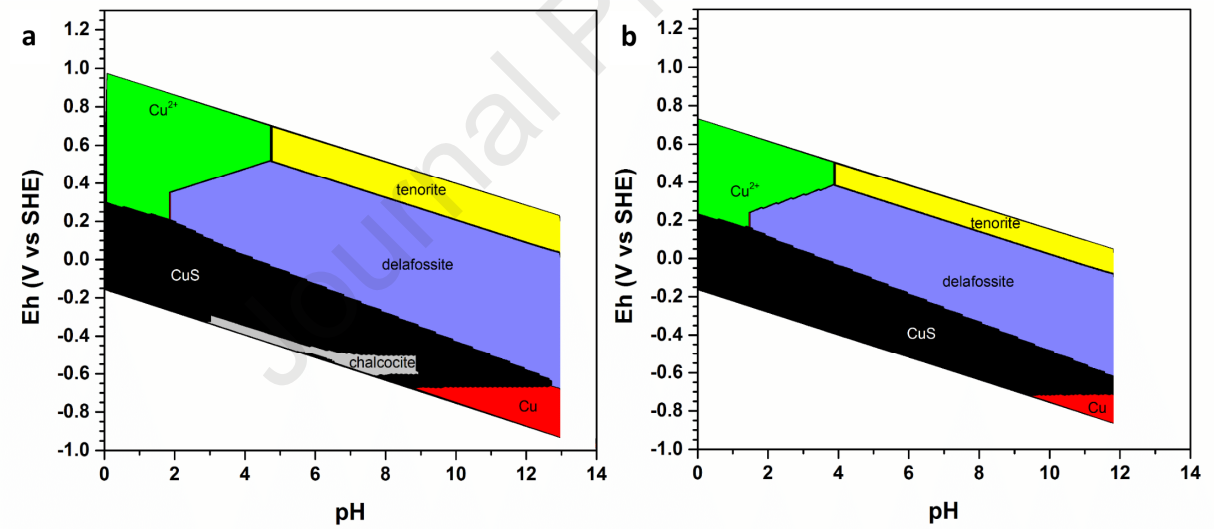

Figure 2 Eh-pH prevalence diagrams presenting Cu-bearing species for [S]=1 10^{-1} mol dm^{-3}, [Cu]=[Fe]=1 10^{-3} mol dm^{-3} at a) 373 K and b) 473 K. The CuS label refers to both covellite and cryptocrystalline CuS prevalence fields.

3.2 Iron-bearing species

In **Figure 3a and 3b**, we can see how the change of concentration from the low to the high values regime affects only slightly the predominance charts, in the case of Fe. The diagram, in both cases, exhibits prevalence of solid phases, the solute species being mainly confined in the oxidising region at

very low pH. As in the case of the diagrams related to the Cu species, one can highlight the wide predominance region of delafossite, occurring within boundaries approximately similar to those shown in the **Figure 1**. This marks the ubiquitous prevalence of delafossite in a wide range of pH values, and under moderately to highly oxidising conditions. Pyrite is the predominant iron-bearing species under reducing conditions, with a predominance field located in almost the same region of covellite's predominance field (**Figures 1a and 1b**). As in that case, the predominance field of the binary sulfide is nested in the predominance field of chalcopyrite. There is no predominance field for metallic iron. The most relevant changes with metal concentration regard some boundary shifts between stability fields. Indeed, at high Eh, we observe the increase of the predominance field of hematite toward low pH when passing from the low to high concentration. Similarly, also the predominance field of delafossite increases.

The **Figures 4a and 4b** highlight the progressive decrease of relevance of the solute species. At 373 K, only Fe^{2+} and $FeHSO_4^{2+}$ still exhibit a predominance field, whereas at 473 K only the Fe^{2+}, predominance field is present in the diagram (at low pH and moderate to highly reducing conditions). In general, a decrease of the number of predominant phases is observed, as in the case of the Cu diagrams (**Fig. 2**). Concerning the solid phases, one can note the disappearance of the field of chalcopyrite, being replaced by the predominance fields of mackinawite, pyrite, hematite and delafossite. The predominance field of delafossite follows the same trend observed in the copper predominance charts shrinking by increasing the temperature from 373 K to 473 K. Nevertheless, delafossite still represents the most predominant species in the compositional field.

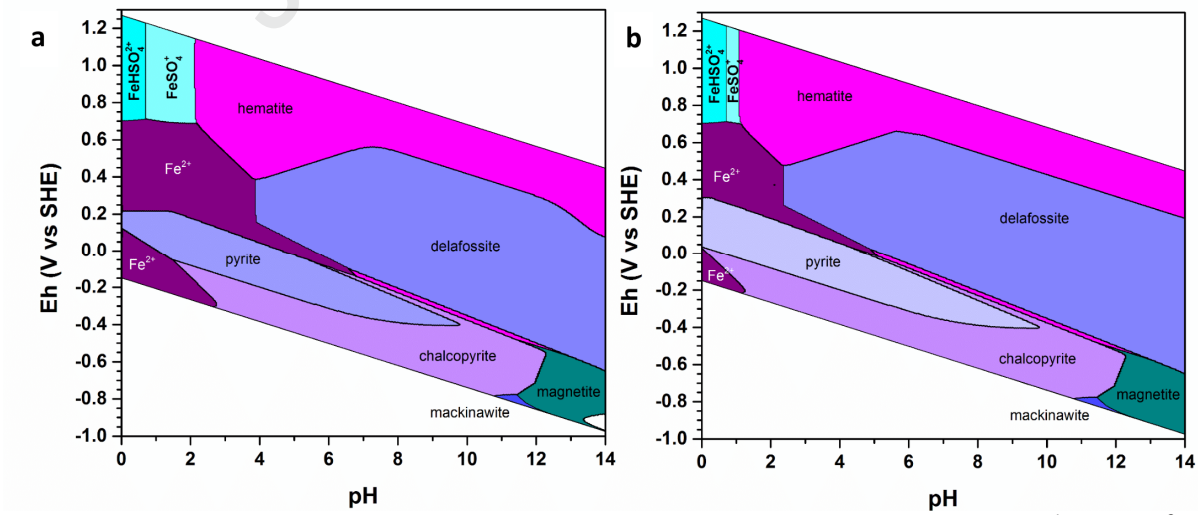

Figure 3 - Eh-pH prevalence diagrams presenting Fe-bearing species at 293 K for [S]=1 10^{-1} mol dm^{-3} a)

[Cu]=[Fe]=1 10^{-6} mol dm^{-3} and b) [Cu]=[Fe]=1 10^{-3} mol dm^{-3}. The small prevalence field at pH ~11, Eh ~-0.75 V in both diagrams pertains to mackinawite.

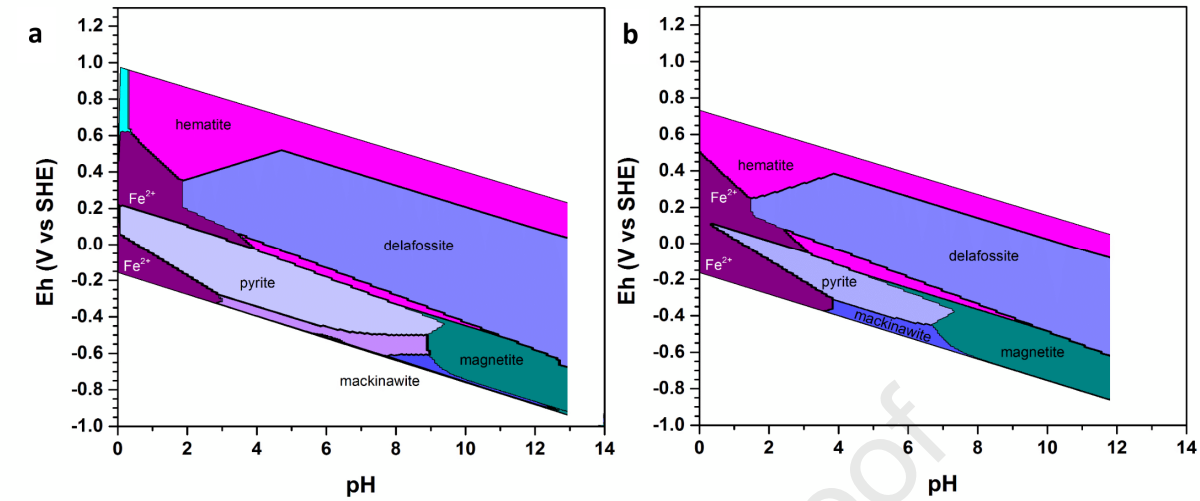

Figure 4 – Eh-pH prevalence diagrams presenting Fe-bearing species for [S]=1 10^{-1} mol dm^{-3}, [Cu]=[Fe]=1 10^{-3} mol dm^{-3} at a) 373 K and b) 473 K. The small prevalence field at pH ~8.5, Eh ~-0.65 V in the a) diagram pertains to mackinawite. The prevalence field at pH <0.5, Eh 0.6-1.0 V in the a) diagram pertains to $FeHSO_4^{2+}$.

4 Discussion

The predominance charts at 293 K of the Cu-bearing phases are like that elsewhere reported for the Cu-S-O-H (Woods et al., 1987; Giaccherini et al., 2016; Huang, 2016). Nevertheless, some relevant differences can be highlighted. Under reducing conditions, the main difference is the emergence of predominance fields for ternary phases. Interestingly, close to the oxidising boundary we found different binary species from the Cu-S-O-H and Fe-S-O-H systems. Moreover, in the Cu-predominance chart of Cu-Fe-S-O-H system $Cu(OH)_2$ substitutes tenorite predominance field (which occurs in the Cu-predominance chart of Cu-S-O-H system, Giaccherini et al. 2016). Similarly, comparing our calculations with Cook and Olive (2012) we can see that the predominance field of hematite extends at high pH and high pE substituting $Fe(OH)_4^-$. These trends can be ascribed to the effect of the competing equilibria on the precipitating phases, which are not considered under the line method approach (Cubiciotti 1988, Huang 2016).

Conversely, in the predominance diagrams hereby reported (**Figures 3a and 3b**) the fields of pyrite, Fe^{2+}, hematite and magnetite have approximately the same shape of the homologous fields provided for the Fe-S system in literature (Vaughan, 2006). Here, the clearest evidence is the absence of a stability field for Fe^{3+}, already described by e.g. Garrels and Christ (1965) and that we ascribed to 1) the effects of the competing equilibria with Cu-bearing species or 2) to an underestimation of the effect of the ligand in the literature. In fact, where the Garrels and Christ's (1965) Eh-pH diagram reports Fe^{3+} we have $FeSO_4^+$ and $FeHSO_4^{2+}$. Even in the case of the Fe predominance diagrams, the presence of large fields attributed to ternary compounds (delafossite and chalcopyrite) is remarkable.

The occurrence of ternary fields in both Figures 1 and 3, as well as that different binary compounds present with respect to Cu-S-O-H and Fe-S-O-H diagrams, point out that the Cu and Fe predominance charts are not "independent". This interdependence of the Cu and Sn predominance charts, for comparison, was not observed for the Cu-Sn-S-O-H system (Giaccherini et al., 2016). In this context, modelling the competing equilibria (a difficult task in an equilibrium line approach) between Cu and Fe bearing species results thus crucial to obtain reliable Eh-pH diagrams.

Regarding the concentration dependent changes in the equilibria, the only noticeable changes concern with the larger region of the diagram exhibited by solid phases at high metal concentrations. This is due to the scarce solubility of oxides, sulfides and sulfates of Cu and Fe. Indeed, we found an almost complete filling of the predominance charts with solid phases for rather low Metal/Sulfur ratios (10^{-2}). Indeed, under these conditions the only ions having a relevant predominance field are Cu^{2+} and Fe^{2+}.

Among the temperature dependent effect on the equilibria, we observed that at high temperature the predominance field of pyrite shrinks, while being partially replaced by the predominance field of magnetite. This agrees with experimental studies on the interconversion between the two minerals (Brothers et al., 1996). These authors, in fact, investigated the alteration of pyrite to magnetite at temperature as low as 90 °C in basic solutions at pH ≥8.5. Chalcopyrite vanishes from the predominance chart at 473 K. Nevertheless, we cannot conclude that this mineral is not stable anymore. Indeed, it is just not a predominant phase in the Eh-pH space. On the other hand, chalcopyrite is a widespread primary mineral and one of the most stable (Fleet, 2006).

Delafossite has by far the largest predominance field. This results in a good agreement with its widespread and ubiquitous natural occurrence. From the data here presented one can conclude that

delafossite is a highly probable product of alteration of pristine Cu-, Fe-bearing phases (or assemblages of isolated Cu and Fe compounds). We should stress that this phase is of marginal interest for corrosion due to the immiscibility gap in the Cu-Fe phase diagram, a fact that limits the number of available Cu-, Fe- bearing alloys. However, delafossite can be again relevant for corrosion science purposes in the case of polyphasic materials which include the two metals isolated. Apparently, delafossite represent a secondary phase of greater relevance in the natural settings, where ternary sulfides, or assemblages of Cu- and Fe-bearing sulfides are very common. We see a clear contiguity between the predominance fields of chalcopyrite, chalcocite and delafossite. Following a vertical line from the predominant field of chalcopyrite towards more oxidising conditions, in fact, we pass from chalcopyrite to delafossite in each of the diagrams. Moreover, at higher temperatures the predominance field of delafossite extends to cover part of the stability field of chalcopyrite at basic pH. Indeed, this agrees with the widespread occurrence of delafossite as secondary mineral product of the alteration of chalcopyrite under oxidative and basic conditions, especially in scarcely reducing hydrothermal environment (Fleet, 2006; Henley and Berger, 2012). We want to stress the fact that such alteration process is rather slow and lead to a passivation of chalcopyrite (Henley et al., 2015). Moreover, when the altered chalcopyrite is kept at room temperature, an extremely slow back-conversion of delafossite in chalcopyrite could be thermodynamically favoured according to specific Eh-pH conditions.

5 Conclusion

The predominance charts hereby reported appear in very good agreement with other Eh-pH diagrams computed by means of the line method in the Cu-S-O-H, Fe-S-O-H and Cu-Fe-S-O-H compositional fields (Cubicciotti, 1988; Pourbaix, 1991; Beverskog and Puigdomenech, 1997; Refait et al., 1998; Beverskog and Puigdomenech, 1999; Cook and Olive, 2012). Among the main differences, different phases are found in both iron and copper charts occurring under oxidising conditions, and, remarkably, the presence of a big predominance field for delafossite. The underestimation of delafossite's predominance field by means of the equilibrium line method is probably due to the difficult treatment of the multielement equilibrium in this theoretical framework (Giaccherini et al., 2016; Huang, 2016). Delafossite is a good candidate for solar cells, cathodes, photocathodes, solar water reduction, environmental remediation. Therefore, theoretical models can anticipate the experimental results giving us a robust basis for future studies on stability and synthesis of these extremely useful materials. Moreover, the plots and their changes according to the temperature explain well the alteration of

chalcopyrite to delafossite in the weathered copper and iron ore deposits. To this aim, the modelling of competing equilibria is crucial, and can be approached straightforwardly with the point by point predominance charts.

Bibliography

Anthony, J.W., Bideaux, R.A., Bladh, K.W., Nichols, M.C., eds. (1997). *Handbook of Mineralogy*. III (Halides, Hydroxides, Oxides). Chantilly, VA, US: Mineralogical Society of America. ISBN 0962209732.Q.

Ball, J.W., Nordstrom, D. 1991. WATEQ4F - User's manual with revised thermodynamic data base and test cases for calculating speciation of major, trace and redox elements in natural waters. U.S. Geological Survey Open-File Report; 91-183: 1-189. https://doi.org/10.3133/ofr91183

Bandy, M.C. 1938. Mineralogy of three sulphate deposits of northern Chile. Amer. Mineral., 23, 669–760.

Benreguia, N., Barnabè, A., Trari, M., 2006. Journal of Sol-Gel Science and Technology, 75, 670-679. https://doi.org/10.1007/s10971-015-3737-x

Berger, E.L., Zega, T.J., Keller, L.P., Lauretta, D.S., 2011. Evidence for aqueous activity on comet 81P/Wild 2 from sulfide mineral assemblages in Stardust samples and CI chondrites. Geochim. Cosmochim. Acta 75, 3501–3513. https://doi.org/10.1016/j.gca.2011.03.026

Beverskog, B., Puigdomenech, I. 1997. Revised Pourbaix Diagrams for Copper at 25 to 300°C. J. Electrochem. Soc. 144(10), 3476-3483. https://doi.org/10.1149/1.1838036.

Beverskog, B., Puigdomenech, I. 1999. Pourbaix Diagrams for the Ternary System of Iron-Chromium-Nickel. Corrosion 55(11), 1077-1087. https://doi.org/10.5006/1.3283945.

Borgheresi, M., Di Benedetto, F., Caneschi, A., Pratesi, G., Romanelli, M., Sorace, L. 2007. An EPR and SQUID magnetometry study of bornite. Phys. Chem. Minerals, 34(9), 609-619, https://doi.org/10.1007/s00269-007-0175-5

Brothers, L.A. , Engel, M.H. , Elmore, R.D. 1996. The late diagenetic conversion of pyrite to magnetite by organically complexed ferric iron. Chem. Geol., 130(1–2), 1-14. https://doi.org/10.1016/0009-2541(96)00007-1

Bykova, E., Dubrovinsky, L., Dubrovinskaia, N., Bykov, M., McCammon, C., Ovsyannikov, S.V., Liermann, H.-P., Kupenko, I., Chumakov, A. I., Rüffer, R., Hanfland M., Prakapenka V. 2016. Structural complexity of simple Fe_2O_3 at high pressures and temperatures. Nature Communications, 7, 10661, https://doi.org/10.1038/ncomms10661

Chuckhov, F.V., Zvyagin, B.B., Gorshov, A.I., Yermilova L.P., Balashova, V.V. 1974. Ferrihydrite. Int. Geol. Rev., 16(10), 1131-1143, DOI: 10.1080/00206817409471766

Cook, W., Olive, R. 2011. Pourbaix diagrams for the iron–water system extended to high-subcritical and low-supercritical conditions. Corrosion Sci.; 55, 326-331, https://doi.org/10.1016/j.corsci.2011.10.034.

Crerar, D.A., Barnes, H.L. 1976. Ore solution chemistry; V, Solubilities of chalcopyrite and chalcocite assemblages in hydrothermal solution at 200 degrees to 350 degrees C. Econ. Geol., 71(4), 772–794. https://doi.org/10.2113/gsecongeo.71.4.772

Cubicciotti, D. 1988. Pourbaix Diagrams for Mixed Metal Oxides - Chemistry of Copper in BWR Water. Corrosion 44(12), 875-880. https://doi.org/10.5006/1.3584959.

Di Benedetto, F., Borgheresi, M., Caneschi, A., Chastanet, G., Cipriani, C., Gatteschi, D., Pratesi, G., Romanelli, M., Sessoli, R. 2006. First evidence of natural superconductivity: covellite. Eur. J. Mineral, 18, 283-287, https://doi.org/10.1127/0935-1221/2006/0018-0283

Díaz-García, A.K., Lana-Villarreal, T., Gómez R. 2015. Sol–gel copper chromium delafossite thin films as stable oxide photocathodes for water splitting. J. Mater. Chem. A 3, 19683-19687. https://doi.org/10.1039/C5TA05227K.

Dubrovinsky, L.S., Dubrovinskaia, N.A. , Mc Cammon, C., Rozenberg, G.Kh., Ahuja, R. , Osorio-Guillen, J.M. , Dmitriev, V. , Weber, H-P. , Le Bihan T. , Johansson B. 2003. The structure of the metallic high-pressure Fe_3O_4 polymorph: experimental and theoretical study. J. Phys. Condens. Matter, 15, 7697–7706.

Fang, J.H., Robinson, P.D. 1970. Crystal structures and mineral chemistry of hydrated ferric sulfates. I. The crystal structure of coquimbite. Amer. Mineral., 55, 1534–1540.

Fleet, M. E. 2006. Phase Equilibria at High Temperatures. Rev. Miner. Geochem., 61(1), 365–419, https://doi.org/10.2138/rmg.2006.61.7

Gablina, I., Semkova, T.A., Stepanova, T., Gor'kova, N. 2006. Diagenetic alterations of copper sulfides in modern ore-bearing sediments of the Logatchev-1 hydrothermal field (Mid-Atlantic Ridge 14°45' N). Lithology Min. Res., 41, 27-44, https://doi.org/10.1134/S0024490206010032.

Garrels, R., Christ, C.L. 1965. Solutions, minerals, and equilibria. Jones and Bartlett Publishers. ISBN 0-86720-148-7

Giaccherini, A., Montegrossi, G., Di Benedetto, F. 2016. Stability of Naturally Relevant Ternary Phases in the Cu–Sn–S system in Contact with an Aqueous Solution. Minerals, 6(3), 79, https://doi.org/10.3390/min6030079.

Goble, R. J. 1985. The relationship between crystal structure, bonding and cell dimensions in the copper sulfides. Can. Mineral., 23(1), 61–76.

Hatert, F. 2004. Occurrence of sulphides on the bornite-idaite join from Vielsalm, Stavelot Massif, Belgium. Eur. J. Mineral., 15(6), 1063-1068, https://doi.org/10.1127/0935-1221/2003/0015-1063.

Helgeson, H.C., Delany, J.M., Nesbitt H.W., Bird, D.K. 1978. Summary and critique of the thermodynamic properties of rock forming minerals. Amer. J. Sci. 278-A.

Henley, R.W. , King, P.L. , Wykes, J.L. , Renggli, C.J., Brink, F.J., Clark, D.A., Troitzsch, U. 2015. Porphyry copper deposit formation by sub-volcanic sulphur dioxide flux and chemisorption. Nat. Geosci., 8, 210-215, https//doi.org/10.1038/NGEO2367

Henley, R.W., Berger, B.R. 2012. Pyrite-sulfosalt reactions and semimetal fractionation in the Chinkuashih, Taiwan, copper–gold deposit: a 1 Ma paleo-fumarole. Geofluids, 12(3), 245-260, https//doi.org/10.1111/j.1468-8123.2012.00367.x

Hu, Q., Kim, D.Y., Yang, W., Yang, L., Meng,Y., Zhang, L., Mao H.-K. 2016. FeO_2 and FeOOH under deep lower-mantle conditions and Earth's oxygen–hydrogen cycles. Nature, 534, 241–244, https://doi.org/10.1038/nature18018

Huang, H.H. 2016. The Eh-pH Diagram and Its Advances. Metals, 6(1), 23, https://doi.org/10.3390/met6010023.

Johnson, J.W., Oelkers, E.H., Helgeson, H.C. 1992. SUPCRT92: A software package for calculating the standard molal thermodynamic properties of minerals, gases, aqueous species, and reactions from 1 to 5000 bar and 0 to 1000°C. Computers Geosci., 18, 899-947, https://doi.org/10.1016/0098-3004(92)90029-Q.

Kang, U., Choi, S.K., Ham, D.J., Ji, S.M., Choi, W., Han, D.S., Abdel-Wahab, A., Park, H. 2015. Photosynthesis of formate from CO_2 and water at 1% energy efficiency via copper iron oxide catalysis. Energy Environ. Sci., 8, 2638-2643, https://doi.org/10.1039/C5EE01410G

Klein, C., Hurlbut, C.S., Dana, J.D. 1985. Manual of mineralogy (after James D. Dana) (20th ed). New York Wiley

Lafuente, B., Downs, R.T., Yang, H., Stone, N. 2015. The power of databases: The RRUFF project. Highlights in Mineralogical Crystallography; 1-30. https://doi.org/10.1515/9783110417104-003.

Lavina, B., Meng, Y. 2015. Unraveling the complexity of iron oxides at high pressure and temperature: Synthesis of Fe_5O_6. Science Advances 1(5), e1400260, DOI: 10.1126/sciadv.1400260

Lavina, B., Dera, P., Kim, E., Meng, Y., Downs, R.T., Weck, P.F., Sutton, S.R., Zhao Y. 2011. Discovery of the recoverable high-pressure iron oxide Fe_4O5. Proc. Nat. Acad. Sci., 108(42), 17281-17285, https://doi.org/10.1073/pnas.1107573108

Long, S.O.J., Powell, A.V., Vaqueiro, P., Hull, S. 2018. High Thermoelectric Performance of Bornite through Control of the Cu(II) Content and Vacancy Concentration. Chem. Mater., 30(2), 456-464, https://doi.org/10.1021/acs.chemmater.7b04436

Manutchehr-Danai M. 2006. "Mechanical translation". In: Dictionary of Gems and Gemmology. Springer, Berlin, Heidelberg (2009) https://doi.org/10.1007/978-3-540-72816-0.

Marquardt, M.A., Ashmore, N.A., Cann, D.P. 2006. Crystal chemistry and electrical properties of the delafossite structure. Thin Solid Films, 496(1), 146-156, https://doi.org/10.1016/j.tsf.2005.08.316

Merlini, M., Hanfland, M. , Salamat, A. , Petitgirard S. , Müller H. 2015) The crystal structures of $Mg_2Fe_2C_4O_{13}$, with tetrahedrally coordinated carbon, and $Fe_{13}O_{19}$, synthesized at deep mantle conditions. Am. Miner., 100(8-9), 2001–2004, https://doi.org/10.2138/am-2015-5369

Miller, T., Wittenberg, J., Wen, H., Connor, S., Cui, Y., Lindenberg A. 2013. The mechanism of ultrafast structural switching in superionic copper(I) sulphide nanocrystals. Nat. Commun. 4, 1369. https://doi.org/1369. 10.1038/ncomms2385.

Mugnier, E., Barnabè, A., Tailhades, P., 2006. Solid State Ionics, 177, 607-622. https://doi.org/10.1016/j.ssi.2005.11.026

Mulafa-Bafubiandi, A. 2006. Characterization of products emanating from conventional and microwave energy roasting of chalcopyrite ($CuFeS_2$) concentrate. Hyperfine Int., 168, 923-928, https://doi.org/10.1007/s10751-006-9398-y.

Parkhurst, D.L., Appelo, C.A.J. 1999. User's Guide to PHREEQC (version 2) — a Computer Program for Speciation, and Inverse Geochemical Calculations. Exch. Organ. Behav. Teach. J.D, 326, https://doi.org/10.3133/wri994259.

Pourbaix, M. 1991. Thermodynamics and Corrosion. In: Ferreira M.G.S., Melendres C.A. (eds) Electrochemical and Optical Techniques for the Study and Monitoring of Metallic Corrosion. NATO ASI Series (Series E: Applied Sciences); 203. https://doi.org/10.1007/978-94-011-3636-5_1.

Prévot, M., Guijarro, N., Sivula, K. 2015. Enhancing the Performance of a Robust Sol–Gel-Processed p-Type Delafossite $CuFeO_2$ Photocathode for Solar Water Reduction. Chem. Sus. Chem., 8, 1359-1367, https://doi.org/10.1002/cssc.201403146

Qiu, P., Zhang, T., Qiu, Y., Shi, X. , Chen, L. 2014. Sulfide bornite thermoelectric material: A natural mineral with ultralow thermal conductivity. Energy Environ. Sci., 7, 4000-4006, https://doi.org/10.1039/C4EE02428A

Raghavan, V. 2004. Cu-Fe-S. J. Phase Eq. Diffusion, 25(5), 450-454, 10.1361/15477030420845

Rais, A., Gismelseed, A.M., Al-Rawas A.D. 2000. Magnetic properties of natural chalcopyrite at low temperature. Materials Letters 46(6), 349-353. 10.1016/S0167-577X(00)00199-3

Read, C.G., Park, Y., Choi, K.S. 2012. Electrochemical Synthesis of p-Type CuFeO2 Electrodes for Use in a Photoelectrochemical Cell. J. Phys. Chem. Letters, 3(14), 1872-1876, https://doi.org/10.1021/jz300709t.

Refait, P.H., Abdelmoula, M., Génin, J.M. 1998. Mechanisms of formation and structure of green rust one in aqueous corrosion of iron in the presence of chloride ions. Corrosion Sci., 40, 1547-1560, https://doi.org/10.1016/S0010-938X(98)00066-3.

Rockett, A.A. 2010. Current status and opportunities in chalcopyrite solar cells. Curr. Opinion Solid State Mater. Sci. 14(6), 143-148. https://doi.org/10.1016/j.cossms.2010.08.001.

Rogers, A. 1913. Delafossite, a Cuprous Metaferrite from Bisbee, Arizona. Am. J. Sci., 35, 290-294, https://doi.org/10.2475/ajs.s4-35.207.290.

Sato, M. 1992. Persistency-field Eh-pH diagrams for sulfides and their application to supergene oxidation and enrichment of sulfide ore bodies. Geochim. Cosmochim. Acta, 56(8), 3133-3156, https://doi.org/10.1016/0016-7037(92)90294-S.

Sheets, W. C., Mugnier, E., Barnabè, A., Marks, T. J., Poeppelmeier, K. R., 2006. Chemistry of Materials, 18, 7-20 https://doi.org/10.1021/cm051791c.

Siebentritt, S. 2017. Chalcopyrite compound semiconductors for thin film solar cells. Curr. Op. Green Sust. Chem., 4, 1-7, https://doi.org/10.1016/j.cogsc.2017.02.001.

Su, J., Wei, Y., Vayssieres, L. 2017. Stability and Performance of Sulfide-, Nitride-, and Phosphide-Based Electrodes for Photocatalytic Solar Water Splitting. J. Phys. Chem. Letters, 8(20), 5228-5238, https://doi.org/10.1021/acs.jpclett.7b00772.

Takata, T., Tanaka, A., Hara, M., Kondo, J.N., Domen, K. 1998. Recent progress of photocatalysts for overall water splitting. Catalysis Today, 44(1–4), 17-26, https://doi.org/10.1016/S0920-5861(98)00170-9

USGS, 2018. Mineral Commodity Summaries. Accessed on 09/30/2020

Vaughan, D.J., 2006. Sulfide Mineralogy and Geochemistry: Introduction and Overview. Rev. Mineral. Geochemistry 61, 1–5. https://doi.org/10.2138/rmg.2006.61.1

Vaughan, D.J. Craig, J.R. 1978. Mineral Chemistry of Metal Sulfides. (Cambridge Earth Science Series), Cambridge (Cambridge University Press), 1978. xvi+ 493pp. https://doi.org/10.1180/minmag.1979.043.325.27

Whiteside, L. S. , Goble, R. J. 1986. Structural and compositional changes in copper sulfide during leaching and dissolution. Can. Mineral., 24(2), 247–258.

Woods, R., Yoon, R.H. , Young, C. 1987. Eh-pH diagrams for stable and metastable phases in the copper-sulfur-water system. Int. J. Mineral Processing, 20, 109-120, https://doi.org/10.1016/0301-7516(87)90020-2.

Highlights

- New thermodynamic modelling in the Cu-Fe-S-O-H system
- Eh-pH at temperature higher than room temperature
- Revised predominance field for ternary phases in the Cu-Fe-S-O-H
- Cu-Fe-S-O-H is not just the sum of Cu-S-O-H and Fe-S-O-H

Declaration of interests

We declare that the authors have not any conflict of interest. Those include relevant financial, personal, political, intellectual or religious interests.